

Adiabatic and Nonadiabatic Charge Transport in Li–S Batteries

Haesun Park,^{†,○} Nitin Kumar,^{†,○} Marko Melander,^{#,▽,○} Tejs Vegge,[#] Juan Maria Garcia Lastra,[#] and Donald J. Siegel^{*,†,‡,§,||,⊥,♯}

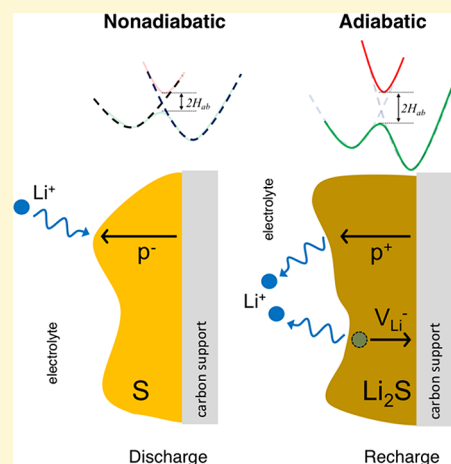
[†]Mechanical Engineering Department, [‡]Materials Science & Engineering, [§]Applied Physics Program, ^{||}Michigan Energy Institute, and [⊥]Joint Center for Energy Storage Research, University of Michigan, Ann Arbor, Michigan 48109-2125, United States

[#]Department of Energy Conversion and Storage, Technical University of Denmark, Fysikvej, Building 309, 2800 Kgs Lyngby, Denmark

[▽]Department of Chemistry, Nanoscience Center, University of Jyväskylä, FI-40014 Jyväskylä, Finland

Supporting Information

ABSTRACT: The insulating nature of the redox end members in Li–S batteries, α -S and Li_2S , has the potential to limit the capacity and efficiency of this emerging energy storage system. Nevertheless, the mechanisms responsible for ionic and electronic transport in these materials remain a matter of debate. The present study clarifies these mechanisms—in both the adiabatic and nonadiabatic charge transfer regimes—by employing a combination of hybrid-functional-based and constrained density functional theory calculations. Charge transfer in Li_2S is predicted to be adiabatic, and thus is well-described by conventional DFT methodologies. In sulfur, however, transitions between S_8 rings are nonadiabatic. In this case, conventional DFT overestimates charge transfer rates by up to 2 orders of magnitude. Delocalized holes, and to a lesser extent, localized electron polarons, are predicted to be the most mobile electronic charge carriers in α -S; in Li_2S , hole polarons dominate. Although all carriers exhibit extremely low equilibrium concentrations, and thus yield negligible contributions to the conductivity, their mobilities are sufficient to enable the sulfur loading targets necessary for high energy densities. Our results highlight the value of methods capable of capturing nonadiabaticity, such as constrained DFT. These techniques are especially important for molecular crystals such as α -S, where longer-range charge transfer events are expected. Combining the present computational results with prior experimental studies, we conclude that low equilibrium carrier concentrations are responsible for sluggish charge transport in α -S and Li_2S . Thus, a potential strategy for improving the performance of Li–S batteries is to increase the concentrations of holes in these redox end members.



INTRODUCTION

The lithium–sulfur (Li–S) system is an emerging, “beyond Li-ion” battery chemistry,^{1–5} with a high theoretical energy density (2199 W h/L) and specific energy (2567 W h/kg),⁵ potential for low cost,² and low toxicity.⁶ Unfortunately, these benefits have not yet been fully realized in practical Li–S cells, largely due to two unmet challenges. These include polysulfide (PS) dissolution/shuttling and the insulating nature of the redox end members (REMs), α -S and Li_2S .² PS dissolution has been widely studied;^{1,2} strategies to suppress dissolution include the use of cathode architectures that physically and/or chemically confine S and PS,^{1,7–11} and substitution of conventional electrolytes with solids, or with those that are non-solvating, or sparingly solvating, for PS.^{3,12–20}

Strategies aimed at suppressing PS dissolution are expected to alter electrochemical reactions in the cathode such that they become localized near the surface of the cathode support, resulting in more solid-state-like behavior.^{3,21} Consequently, transport mechanisms involving solid-state S and Li_2S are expected to play an important role in this “surface mediated”

regime. Transport limitations involving both S and Li_2S REM are possible, as both phases are insulators with large bandgaps.^{22,23}

Regarding Li_2S , the formation of this compound during discharge can mimic the behavior of Li_2O_2 in Li/ O_2 cells. Earlier studies on the Li/ O_2 system have shown that the insulating nature of the Li_2O_2 discharge product can limit capacity and increase overvoltages during charging.^{24–32} Thus, by limiting PS solubility in Li–S cells one risks trading the PS dissolution problem for a transport problem arising from cathode passivation. Passivation can also be a concern in Li–S cells in the charged state: Oxidation of Li_2S during charging generates sulfur, which is also a poor electronic conductor. Transport through S may also be an important consideration in optimizing the initial distribution and loading of S in the cathode, to maximize S utilization. In total, transport limitations

Received: November 2, 2017

Revised: December 19, 2017

Published: December 20, 2017

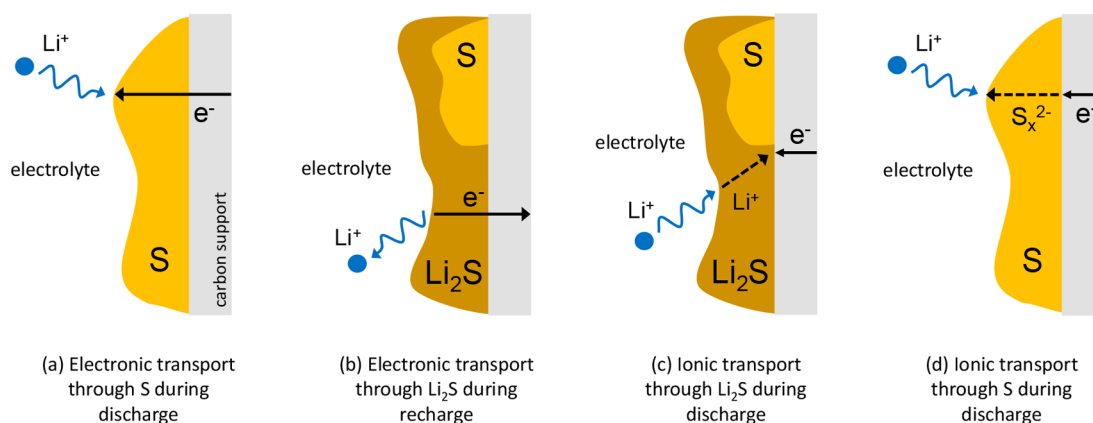


Figure 1. Possible electronic and ionic transport processes in the cathode of a Li–S cell during discharge or charging. Yellow represents sulfur, brown represents Li_2S , and gray represents the cathode support (assumed to be carbon).

in Li–S cells may pose challenges that are double those of the Li/ O_2 system, because in the former chemistry *both* REMs are electronic insulators.

Figure 1 illustrates plausible electronic and ionic transport mechanisms that may occur in the cathode of a Li–S cell during discharge or charge. Figure 1a demonstrates electronic transport through a sulfur film that covers a carbon cathode support. Reduction of S_8 to S_x^{2-} requires charge transport from the current collector to the reaction site on the S surface. This could result in solid-state film growth of Li_2S at the reaction site, or the formation of soluble PS that ultimately precipitates as Li_2S elsewhere in the cell.

An alternative scenario occurs when S does not completely cover the carbon support. This creates a three-phase boundary between the electrolyte, S, and the support in the fully or partially charged state.³³ Consequently, facile electronic charge transport would occur (at least initially) through the conductive support, and not through insulating S. However, deposition of Li_2S as discharge progresses can ultimately bury the three-phase interface, as depicted in Figure 1b. In this case, electronic transport through insulating Li_2S is necessary during charging.

The need for long-range electronic transport can be minimized if rapid ionic transport through Li_2S is possible. For example, Figure 1c shows that Li_2S or PS can grow at buried $\text{Li}_2\text{S}/\text{S}$ or $\text{Li}_2\text{S}/\text{support}$ interfaces if Li_2S conducts Li ions. Similarly, transport of reduced S ions, S_x^{2-} , through S (or Li_2S) could allow Li_xS_y formation on the surface of these phases, Figure 1d.

Understanding the transport properties of the S and Li_2S REMs is a prerequisite for the development of rational strategies to improve the capacity, efficiency, and cycle life of Li–S batteries. Nevertheless, transport mechanisms in these compounds have not been widely studied, especially in the case of S.^{34–37} While a few studies exist for Li_2S , consensus regarding the dominant charge-carrying species has been slow to emerge. For example, Kang et al. reported that the dominant charge carriers in Li_2S are negative Li and positive S vacancies, based on calculations performed at the hybrid functional level of theory. The most likely electronic charge carrier was predicted to be the electron polaron, which localizes on sulfur ions.²² In contrast, using a similar level of theory, Mukherjee et al. argue that hole polarons are formed on sulfur ions in Li_2S and, together with negative Li vacancies, serve as lowest-energy charge carriers.³⁷ Moradabadi and co-workers found that the dominant charge carriers were Li vacancies and Li interstitials,

based on calculations employing a semilocal functional.³⁵ (Li interstitials were not considered in refs 22 and 37.) Finally, Mukherjee et al. reported that the main charge carriers in metastable²³ Li_2S_2 (based on a hypothetical crystal structure) are hole polarons and negatively charged Li vacancies.³⁶

More generally, nearly all prior studies on charge migration/hopping in cathode materials (typically involving localized electronic carriers such as polarons)^{34–36} have been performed assuming these are *adiabatic* processes. Within the adiabatic picture, the Born–Oppenheimer approximation is assumed to hold, and it is thus sufficient to map the minimum energy pathway (MEP) along a single, smoothly varying electronic ground state, using, for example, the nudged elastic band (NEB) method (i.e., orange curve in Figure 2).^{38–40} The rate constant can then be derived from the energy at the saddle point along the MEP using (harmonic) transition state theory.

However, charge transfer processes can also be electronically *nonadiabatic* if the ground and excited states become sufficiently close in energy or cross each other (i.e., a conical intersection) and are thus weakly coupled. Instead of a smooth

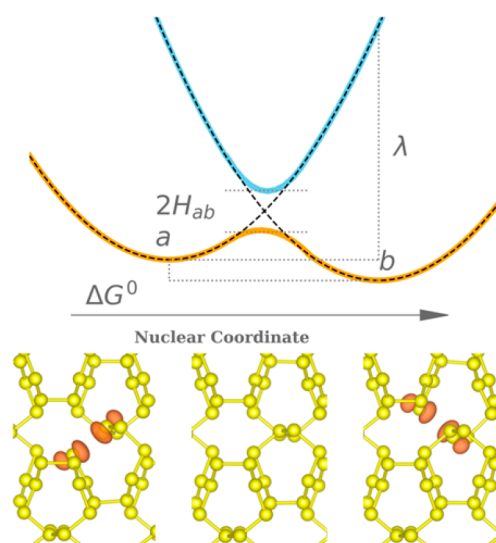


Figure 2. Schematic representation of charge transfer in Marcus theory. The orange (blue) solid line is the adiabatic ground (excited) state while the dashed lines are the two diabatic states describing the initial (a) and final (b) states. H_{ab} is the coupling constant, ΔG° is the free energy change of the reaction, and λ is the reorganization energy.

MEP, the resulting nonadiabatic charge transfer event exhibits an abrupt change and a cusp in the energy along the reaction coordinate, as shown with the dashed curves in Figure 2. In such cases, it is natural to work with *diabatic* electronic states. These states are not ground states, but retain their chemical and physical character independent of the geometry. Here, the rate constant, $k_{a \rightarrow b}$, can be expressed using Marcus theory^{41–43}

$$k_{a \rightarrow b} = \frac{2\pi}{\hbar} \frac{|H_{ba}|^2}{\sqrt{4\pi k_B T \lambda}} \exp\left[-\frac{(\Delta G^\circ + \lambda)^2}{4k_B T \lambda}\right] \quad (1)$$

where $H_{ba} = \langle b|\hat{H}|a\rangle$ is the coupling constant (a represents the donor/initial state and b the acceptor/final state), ΔG° is the reaction free energy between states a and b, and λ is the reorganization free energy. Nonadiabatic behavior is expected to occur in materials where large hopping distances must be traversed to achieve macroscopic charge transfer. This scenario exists in sulfur for hopping between S_8 rings. For such a nonadiabatic reaction, H_{ba} is generally small, and can suppress the hopping rate significantly, eq 1.

The goal of the present study is to elucidate charge transport mechanisms in the S and Li_2S REMs in Li–S batteries, while carefully accounting for the (non)adiabatic nature of these processes. The calculated transport rates are used to estimate the theoretical maximum loadings (i.e., limiting film thicknesses) for S and Li_2S that are consistent with practical discharge rates. More specifically, we separately examine the ionic and electronic conductivity resulting from the formation and migration of ionic and electronic carriers in these two materials. The equilibrium concentrations of several plausible charge carriers and their respective adiabatic mobilities were evaluated at the hybrid functional level of theory,^{44,45} using a tuned fraction of exact exchange.³⁰ Subsequently, nonadiabatic effects were examined using the constrained DFT formalism (cDFT). The combination of these approaches allows for a rigorous understanding of how transport phenomena in Li–S cathodes can limit battery performance.

In sulfur, our cDFT calculations indicate that transitions between S_8 rings are nonadiabatic. This result highlights the importance of going beyond the Born–Oppenheimer approximation, which in this case erroneously overestimates charge transfer rates by up to 2 orders of magnitude, even when used in conjunction with hybrid functionals. Delocalized holes, and, to a lesser extent, localized electron polarons (p^-), are predicted to be the most mobile electronic charge carriers. All carriers in sulfur exhibit extremely low equilibrium concentrations, and thus yield negligible contributions to the conductivity. Nevertheless, the mobilities of free holes and p^- are sufficient to enable the sulfur loading targets necessary for high energy densities. Based on the calculated mobility, and assuming a C/5 discharge rate, we estimate that p^- can transit S films with a thickness of approximately $\sim 100 \mu\text{m}$. The diffusion length for free holes is much larger, $\sim 1 \text{ m}$. These thicknesses exceed the JCESR S loading target of $6 \text{ mg}/\text{cm}^2$,^{2,46,47} which correspond to a S film with an average thickness $30 \mu\text{m}$.

In the case of Li_2S , positively charged Li interstitials and negatively charged vacancies are the dominant ionic carriers. The Li vacancy is most mobile of these carriers, with an activation energy of 0.32 eV . The most prevalent electronic carriers are hole polarons; however, these carriers are predicted to have a high formation energy (1.95 eV) and extremely low equilibrium concentrations. Despite its low concentration, the hole polaron is highly mobile, with a maximum migration

length of $\sim 40 \text{ nm}$ at a charging rate of C/5. In contrast, the equivalent migration length for Li vacancies is much smaller, $\sim 240 \mu\text{m}$. Importantly, the migration lengths for both carriers surpass the projected maximum thickness ($50 \mu\text{m}$) of a Li_2S film formed upon discharge (assuming an initial sulfur loading equal to the JCESR target).

METHODOLOGY

The formation energies and adiabatic mobilities of various charge carriers were evaluated using density functional theory as implemented in the Vienna *ab initio* simulation package (VASP).^{48,49} The simulation cells consisted of the conventional unit cell for α -S (128 atoms), and a 96-atom supercell constructed from a $2 \times 2 \times 2$ replication of the Li_2S unit cell. The unit cells for both materials are shown in Figure 3. Calculations on the bulk properties of S and Li_2S were reported earlier.²³

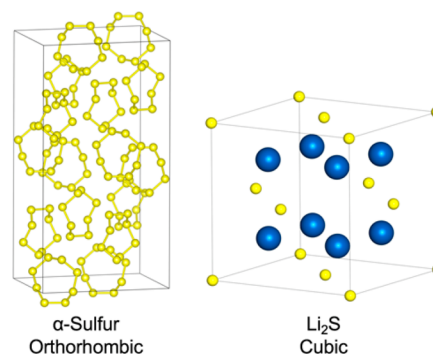


Figure 3. Crystal structures of α -S and Li_2S . Blue and yellow spheres represent Li and S atoms, respectively.

The internal degrees of freedom for both supercells were relaxed to a force tolerance of $0.04 \text{ eV}/\text{\AA}$ (α -S) and $0.01 \text{ eV}/\text{\AA}$ (Li_2S). The dimensions of the α -S supercell were previously calculated⁵⁰ using the vdW-DF functional; the following lattice constants were obtained: $a = 10.33 \text{ \AA}$, $b = 12.76 \text{ \AA}$, and $c = 24.45 \text{ \AA}$. The present defect calculations are to be performed using hybrid functionals, which do not account for van der Waals interactions between S_8 rings in α -S. Therefore, the lattice constants of α -S were fixed to the experimental lattice constants,⁵¹ $a = 10.46 \text{ \AA}$, $b = 12.87 \text{ \AA}$, and $c = 24.49 \text{ \AA}$. The lattice constant for Li_2S was determined by fitting total energies and volumes to the Murnaghan equation of state⁵² using the HSE $_{\alpha}$ functional (described below). The calculated lattice constant, 5.68 \AA , is well matched to the experimental value,⁵³ 5.69 \AA . K-point sampling was performed at the Γ -point for α -S and using two irreducible k-points for Li_2S . The projector-augmented wave (PAW) scheme^{54,55} was used to treat core–valence electron interactions. All calculations were spin-polarized with planewave cutoff energies of 450 eV (α -S) and 500 eV (Li_2S).

A total of 18 (α -S) and 24 (Li_2S) distinct defects were studied. These defects were considered both as charged and neutral species, and were composed of vacancies, interstitials, and polarons. Formation energies were evaluated for all symmetry-distinct sites. For Li_2S , Frenkel and Schottky defects were also investigated.

Earlier studies have shown that self-interaction errors present in semilocal functionals can negatively impact the accuracy of these methods when applied to defects that are expected to exhibit localized charge distributions, such as polarons.^{56–58} To minimize these errors, the Heyd–Scuseria–Ernzerhof (HSE)^{44,45} screened hybrid functional was used with the fraction of exact exchange, α , set to 0.48 (HSE $_{48}$). Figure S1 shows the bandgap of Li_2S calculated as a function of α . At $\alpha = 0.48$ the calculated Li_2S bandgap (5.28 eV) matches closely the value obtained from many-body G_0W_0 (5.27 eV)²³ theory. A similar approach has been used³⁰ to examine charge transport in several peroxides and superoxides.^{30,34,59–61}

Table 1. Calculated Defect Formation Energies (E_f), Equilibrium Concentrations (C), Hopping Barriers (E_b), Reorganization Energies (λ), Coupling Integrals (H_{ab}), Electronic Transmission Coefficients (κ), Rate Constants (k), Mobilities (μ), and Conductivities (σ) for α -S and Li_2S ^a

defect type	E_f (eV)	C (cm^{-3})	adiabatic E_b (eV)	diabatic E_b (eV)	λ (eV)	H_{ba} (eV)	κ	k (s^{-1})	μ ($\text{cm}^2/(\text{V s})$)	σ (S/cm)
α -S										
p^- (intraring)	2.36	9×10^{-18}	0.11	0.07	0.45	0.19	1.0	2×10^{11}	3×10^{-3}	4×10^{-39}
p^- (inter-ring)	2.36	9×10^{-18}	0.42	0.38	1.54	1×10^{-3}	0.012	4×10^4	2×10^{-7}	3×10^{-43}
p^+ (intraring) ^c				0.00 ^c	0.18	0.09				
p^+ (inter-ring) ^c				0.023	0.09	1×10^{-5}	9×10^{-6}	4×10^6		
delocalized hole									$1-10^{\text{ed}}$	$5 \times 10^{-19\text{ed}}$
S_7^-	2.23	2×10^{-15}	0.55					5×10^3	3×10^{-10}	7×10^{-44}
S_9^+	2.23	3×10^{-17}	1.62					6×10^{-15}	3×10^{-28}	1×10^{-63}
S_6^+	2.23	6×10^{-16}								
S_7^+	2.25	1×10^{-15}	1.20					7×10^{-8}	3×10^{-21}	5×10^{-55}
Li_2S										
p^+	1.95	4×10^{-11}	0.08	0.03	0.53	0.14	1.0	6×10^{10}	2×10^{-1}	2×10^{-30}
p^-				0.20	1.21	0.11	1.0	4×10^8		
V_{Li}^-	0.84	3×10^8	0.32					4×10^7	1×10^{-6}	6×10^{-17}
Li^+	0.84	1×10^8	0.52					2×10^4	1×10^{-9}	1×10^{-20}
F_{Li}	1.22	1×10^2								
F_{S}	1.45	2×10^{-2}								
Sch	2.36	1×10^{-17}								
Li_2O_2										
p^+	0.95	1×10^7	0.42					$7 \times 10^{3\text{b}}$		5×10^{-20}
V_{Li}^-	0.93	7×10^7	0.36					$1 \times 10^{5\text{b}}$	6×10^{-9}	9×10^{-19}
Na_2O_2										
p^+	0.9	1×10^7	0.47					$5 \times 10^{2\text{b}}$		1×10^{-20}
V_{Na}^-	1.06	3×10^4	0.42					$6 \times 10^{3\text{b}}$	9×10^{-10}	5×10^{-20}

^aPrior calculations on Li_2O_2 (ref 30) and Na_2O_2 (ref 61) are also shown for comparison. ^bCalculated from published activation energy (E_b) assuming room temperature (300 K) and an attempt frequency of 10^{13} s^{-1} (refs 30 and 61). ^cThe hole polaron in α -S is kinetically unstable and spontaneously delocalizes. ^dExperimental data from refs 74–78.

carriers: positive S interstitials (S_i^+ , equivalent to a positively charged S_9 ring, S_9^+), double S vacancies ($2\text{V}_\text{S}^+ = \text{S}_6^+$), and single S vacancies ($\text{V}_\text{S}^+ = \text{S}_7^+$). The formation energies for these carriers are 2.23, 2.23, and 2.25 eV, respectively. The hole polaron (p^+) has a slightly higher formation energy of 2.45 eV. The defect with the lowest formation energy overall is the neutral S double vacancy ($2\text{V}_\text{S} = \text{S}_6$), with $E_f = 0.18$ eV. (Delocalized holes also play an important role in transport in α -S, and will be discussed separately below.)

We note that the formation energies for all of the charged defects considered are very high (greater than 2.2 eV); consequently, the concentrations of these carriers under equilibrium conditions will be negligible, as summarized in Table 1. For example, the highest concentration predicted for a charged defect is $2 \times 10^{-15} \text{ cm}^{-3}$ for S_7^- . To place this value in context, the concentration of carriers in undoped Si (which is a poor conductor at room temperature) is 25 orders of magnitude higher.⁷⁹ In contrast, the neutral sulfur vacancy, V_S , has a relatively high concentration of $2 \times 10^{16} \text{ cm}^{-3}$, yet it will not contribute to conductivity due to its neutrality.

Regarding the properties of polarons, the magnetization densities for both electron and hole polarons in α -S are shown in Figure 5. In the case of p^- , the extra electron localizes on one of the S–S bonds on a S_8 molecule. The shape of the occupied orbital suggests an antibonding σ^* state. The presence of the additional electron results in an elongation of the bond from 2.05 to 2.65 Å. A comparison of the energies of localized (p^-) and delocalized electrons shows that localization is preferred by 0.42 eV. This is in very good agreement with a prior drift

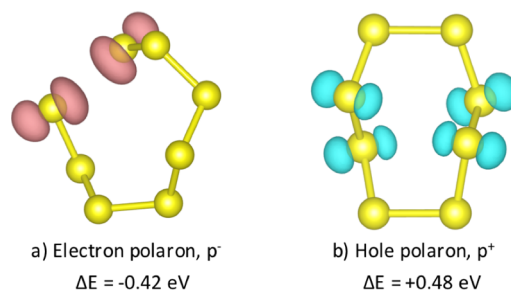


Figure 5. Magnetization density for (a) electron (p^-) and (b) hole (p^+) polarons in α -S. For clarity, only the S_8 molecule where the polaron localizes is shown. The localization energy, $\Delta E = E_{\text{localized}} - E_{\text{delocalized}}$, is shown below each polaron type.

mobility experiment⁸⁰ that determined the p^- binding energy to be 0.48 eV.

In contrast to the more localized nature of the electron polaron, the hole polaron (p^+) localizes on two pairs of S–S bonds, Figure 5b, located on opposite sides of a S_8 ring. This results in a slight distortion of the ring, wherein the S–S–S bond angles change from $\sim 107^\circ$ to $\sim 102^\circ$, with insignificant change in the S–S bond lengths. We find that the p^+ are unstable with respect to the delocalized state by 0.48 eV.

Charge Carrier Mobility in α -S. The low equilibrium concentrations of charge-carrying defects in α -S suggest that even a barrierless charge hopping process will result in an extremely low conductivity. However, this conclusion assumes that equilibrium concentrations are established. In practice, however, battery operation involves the relatively rapid growth

and decomposition of the REM at near-ambient temperatures. Such conditions may generate much higher, nonequilibrium carrier concentrations. This possibility motivates an examination of the mobility of charge carriers in α -S.

In the adiabatic limit, mobility can be estimated from the migration energy barriers of the individual defects, calculated using the CI-NEB method.³⁸ Figure 6a shows the minimum

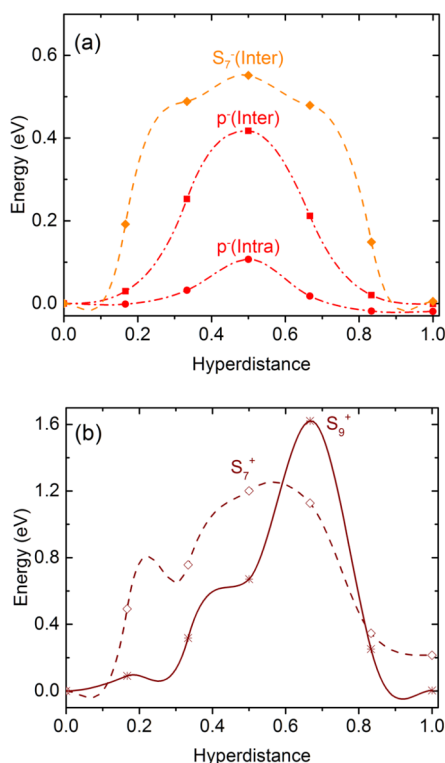


Figure 6. Activation energies (calculated with the CI-NEB) associated with the migration of dominant (a) negative and (b) positive charge carriers in α -S. “Inter” refers to hops between adjacent sulfur rings, while “Intra” refers to hops within the same ring. All hops in panel b are inter-ring hops.

energy pathways for the highest-concentration negatively charged defects in α -S. For the ionic carriers, hopping was examined only between adjacent S_8 rings, i.e., inter-ring hops, as these hopping mechanisms are anticipated to be rate-limiting due to their longer hopping distances (compared to intraring hops). In the case of S_7^- , migration occurs with an activation energy of 0.55 eV. By way of comparison, this value is 0.1–0.2 eV larger than the migration barrier for negative vacancies in Li_2O_2 and Na_2O_2 , Table 1.^{30,61} Hopping of the electron polaron, p^- , has a slightly smaller inter-ring hopping barrier of 0.42 eV. Polaron hopping was also examined within a single S_8 molecule. These intraring hops have the lowest activation energy of any carrier considered in α -S, 0.11 eV. This value agrees well with the experimentally obtained value of 0.167 eV (assuming experiments refer to intraring hops).⁸⁰ Nevertheless, we emphasize that hopping via intraring processes alone cannot lead to charge transport over macroscopic distances; inter-ring processes constitute the rate-limiting steps.

Figure 6b illustrates the adiabatic hopping barriers for the two stable positively charged defects, S_7^+ and S_9^+ . (Migration of p^+ was not considered due the fact that it is unstable with respect to the delocalized state.) S_9^+ exhibits a relatively high

activation energy of 1.62 eV, while the predicted barrier for S_7^+ is 1.20 eV.

The calculations presented above have assumed adiabaticity of the charge transfer events. The validity of this assumption is assessed here using cDFT. All cDFT results are collected in Table 1, and compared with the adiabatic data previously described. We first discuss the behavior of the electron polaron (p^-) in α -S, which our HSE $_{\alpha}$ calculations find to be stable (relative to a delocalized electron). The hopping barriers from cDFT for intra- and inter-ring electron polaron hops are 0.07 and 0.38 eV, respectively. As can be seen in Table 1, the agreement between HSE-NEB and cDFT-Marcus barriers is very good—the barriers predicted by the different methods differ by less than 40 meV.

Although the good agreement in migration barriers for p^- might suggest that all hops can be characterized as adiabatic, the value of the transmission coefficient, κ , suggests otherwise. More specifically, only the intraring process has a κ value of 1, which is indicative of adiabatic behavior. In contrast, the transmission coefficient for the inter-ring hop is very small ($\kappa = 0.012$), indicating that diabatic effects are important. The nonadiabaticity of inter-ring p^- transfer is due to the weak coupling between the initial and final states ($H_{ba} = 1 \times 10^{-3}$), which is consistent with the relatively large distance, 3.4 Å, between them. In total, inter-ring electron transfer exhibits a diabatic hopping rate constant k of $4 \times 10^4 \text{ s}^{-1}$. This value is approximately 2 orders of magnitude smaller than the equivalent adiabatic rate constant. The values reported in Table 1 for the hopping rate, mobility, and conductivity of electron polarons account for the nonadiabaticity described above. The mobility estimated for intraring p^- migration is $3 \times 10^{-3} \text{ cm}^2/(\text{V s})$, which is in close agreement with that determined in drift mobility experiments ($6.2 \times 10^{-4} \text{ cm}^2/(\text{V s})$), assuming the same hopping mechanism is probed experimentally.⁸⁰

Regarding hole polarons, the cDFT calculations confirm the results from the previously described hybrid functional calculations, indicating that p^+ are unstable. For example, the barrier for an intraring hop of p^+ vanishes when charge is constrained to reside on two neighboring S atoms. This suggests that positive charge is delocalized at least across a single sulfur ring. However, hole polaron transfer to an adjacent ring is predicted to be slow and clearly nonadiabatic, as inferred from the transmission coefficient value $\kappa \sim 10^{-6}$. Nevertheless, the inter-ring hole polaron transfer barrier of 23 meV is smaller than thermal energy at room temperature, and therefore the hole polaron in α -S is expected to delocalize over distances larger than that of a single S_8 ring. This hypothesis was confirmed using nonadiabatic Ehrenfest nuclear–electron dynamics, as detailed in the Supporting Information. As shown in Figure S2, the Ehrenfest dynamics simulation predicts that a localized hole on a single S_8 ring becomes delocalized on p-type orbitals across all 128 S atoms in the simulation cell. This delocalization occurs within 10 fs, and without changes to the S–S bond lengths, pointing to a band conduction mechanism for hole transport, rather than localized (polaronic) hopping.

Conductivity in the bandlike regime is mainly governed by the scattering of charge carriers by impurities and vibrational modes of the crystal, which in turn determine their mean free path (or, equivalently, the mean free time, τ); thus, transition state and Marcus theory are not applicable. In principle, the impact of impurities on the mean free path could be obtained

Table 2. Charge Carrier Diffusion (L) and Drift (L_d) Lengths (in μm) for the Predominant Charge-Carrying Species in α -S and Li_2S as a Function of Rate

defect type	C/10		C/5		1C	
	L	L_d	L	L_d	L	L_d
α -S						
p^- (inter-ring)	131	258	93	182	41	82
S_7^-	5	10	4	7	2	3
S_7^+	0	0	0	0	0	0
S_9^+	0	0	0	0	0	0
delocalized holes		10^6		10^6		10^5
Li_2S						
V_{Li}^-	345	678	244	479	109	214
Li^+	11	22	8	16	4	7
p^+	52 000	100 000	37 000	73 000	17 000	33 000

through *ab initio* methods, by combining the nonequilibrium Green's function (NEGF) formalism with DFT.⁸¹ Within this method, it is possible to derive the transmission coefficient due to scattering from each impurity type. Combining these data with the impurity concentration yields the contribution of the impurities to the mean free path. Although the presence of impurities in molecular crystals can reduce carrier mobility significantly (e.g., up to 2 orders of magnitude in pentacene⁸²), the mean free path in these systems is most strongly influenced by scattering from the vibrational modes of the crystal, in particular from the acoustic modes.^{77,83} These low-frequency modes are derived from intermolecular forces. In principle, scattering from vibrations could be characterized through an exhaustive analysis of the electron–phonon coupling;^{83,84} however, accurately describing weak intermolecular interactions (and their associated low-frequency modes) remains a significant challenge, and is not practical at present. Recombination of carriers is another feature that complicates the study of mobility in α -S. As we discuss below, holes move much faster than electrons in α -S (due to band conduction of the former versus hopping for the latter), making the impact of their recombination to the conductivity non-negligible.⁷⁴

Conductivity and Diffusion Length in α -S. As expected from the extremely low equilibrium concentrations of charged defects, the conductivity of α -S arising from hopping mechanisms (which are generally slow processes) is negligible, Table 1. For example, the inter-ring migration of electron polarons, p^- , is the process with the highest hopping-like conductivity of those that contribute to long-range transport. Nevertheless, the value calculated for its conductivity, $\sigma = 3 \times 10^{-43}$ S/cm, is extremely small. Similarly, the highest hopping-type conductivity attributed to positive carriers is also vanishingly small, and arises from vacancy migration, $\text{V}_{\text{S}}^+ = \text{S}_7^+$, with $\sigma = 5 \times 10^{-55}$ S/cm.

However, we have shown that holes in α -S are delocalized and thus migrate via a band conduction mechanism, which is faster than any hopping process. As previously mentioned, analysis of the band conductivity for charge carriers in molecular crystals is a nonaccessible quantity with current *ab initio* methods. Conversely, the experimental mobility of holes in α -S has been measured through drift experiments, and is in the range $\mu = 1\text{--}10$ $\text{cm}^2/(\text{V s})$,^{74,76,77,85} at 300 K. This value is 7 orders of magnitude larger than for any of the hopping mechanisms considered here. Experiments also show that the hole mobility decays with temperature as $\mu \propto T^{-n}$ with $n = 1.6, 1.1,$ and 1.7 in the [100], [010], and [001] directions, respectively.⁸⁵ This is also consistent with a band conduction

model, where the mobility is expected to decay as $\mu \propto T^{-1.5}$ due to scattering from acoustic modes (for optical modes $\mu \propto T^{-0.5}$).⁸⁶

The calculated diffusivities (Table S1) and mobilities were used to establish the migration lengths for charge carriers in α -S. (In the case of delocalized holes, the experimental mobility was used.) These lengths provide an upper bound for the thickness of a S film (i.e., maximum S loading) that can be traversed by these carriers during cell operation at a given C-rate. Assuming a uniform film of α -S with density $\rho_{\alpha\text{-S}} = 2$ g/cm^3 , a loading target⁴⁷ of 6 mg/cm^2 results in a S film with a thickness of 30 μm . Based on the mobility data shown in Table 1, and assuming C-rates (discharge durations) of 1C (3600 s), C/5 (18 000 s), and C/10 (36 000 s), Table 2 summarizes the maximum diffusion lengths, $L = \sqrt{Dt}$, for the dominant hopping-type carriers in α -S: p^- , S_7^- , S_7^+ , and S_9^+ . The maximum diffusion lengths for p^- are 131, 93, and 41 μm for rates of C/10, C/5, and 1C, respectively, assuming inter-ring hopping between S_8 molecules. This suggests that polarons in α -S have sufficient mobility to traverse typical film distances corresponding to the JCESR target S loading. In contrast, the diffusion lengths of the dominant ionic species (S_7^- , S_7^+ , and S_9^+) are all well below the thickness target.

The estimates for the diffusion lengths provided above are based on diffusion in the presence of a concentration gradient. Alternatively, in the presence of an electric field, the drift length, L_d , of a charged species is a more relevant measure of a charge carrier's typical transport length. L_d is given in terms of the mobility, μ : $L_d = \sqrt{\mu Vt}$. Here, V is the voltage drop across the S film, for which we adopt 0.1 V as a plausible value, and t is the time. With these assumptions, our calculations reveal the drift lengths of the hopping-type carriers are roughly double their diffusion lengths, Table 2. Despite this increase, only p^- have sufficient mobility to transit the targeted film thickness. Application of the drift length analysis to delocalized holes in α -S, Table 2, shows that the high mobility of these carriers results in extremely long drift lengths, on the order of 0.1–1 m.

The preceding discussion indicates that the mobility of delocalized holes and p^- are sufficient to enable high S loadings (and high capacity) in Li–S cells. Nevertheless, the experimental conductivity of α -S has been reported to be extremely small, $\sim 5 \times 10^{-19}$ S/cm.⁷⁸ Taken together, these data—sufficient mobility, but poor conductivity—point to low carrier concentrations as the primary obstacle to effective charge transport in α -S. (For example, the large bandgap for α -S suggests that the concentration of free holes at room

temperature will also be very small.²³) In an earlier study, we explored electrical conductivity limitations in Li_2O_2 in the related $\text{Li}-\text{O}_2$ system. There, a cathode conductivity of 10^{-11} S/cm was suggested as a target for achieving efficient operation.³⁰ Adopting that value here, and using the calculated mobility for p^- , a carrier concentration of 10^{15} cm^{-3} is required to achieve the conductivity target. This concentration is 33 orders of magnitude larger than the equilibrium p^- concentration listed in Table 1. Similarly, for delocalized holes, the experimental conductivity and mobility data suggest that an increase in carrier concentration of approximately 8 orders of magnitude is required. Thus, strategies for improving transport in α -S should target increasing the concentrations of free holes and/or electron polarons. In principle, such increases could be achieved through electrolyte additives that are reversibly incorporated as dopants into α -S during recharge (ref 91), or through interfacial effects.

Intrinsic Defects in Li_2S . Figure 7 shows defect formation energies in Li_2S . The predominant defect species, i.e., those

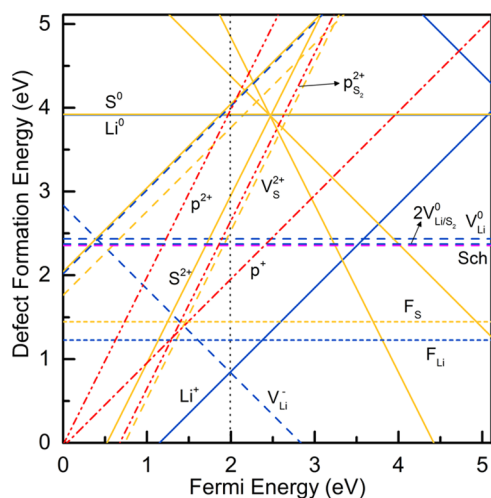


Figure 7. Calculated formation energies for defects in Li_2S . Yellow lines represent ionic defects on the S sublattice, blue lines correspond to ionic defects on the Li sublattice, and red lines refer to polarons. Solid lines are interstitials, while dashed lines represent vacancies. Frenkel defects are identified with the symbols F_S and F_{Li} ; Schottky defects are identified with magenta lines and the symbol “Sch”. The vertical dotted line indicates the position of the Fermi level.

having the lowest formation energies, are the negatively charged lithium vacancy (V_{Li}^-), and the positively charged lithium interstitial (Li^+), both having formation energies of 0.84 eV. The corresponding equilibrium concentrations are 3×10^8 and $1 \times 10^8 \text{ cm}^{-3}$, respectively; these values are 2 orders of magnitude lower than the carrier concentration in undoped Si.⁷⁹ The lowest-energy neutral defect is the Li Frenkel pair (composed of a Li interstitial-vacancy pair), with a formation energy of 1.23 eV.

Our prediction that V_{Li}^- and Li^+ are the highest-concentration equilibrium charge carriers in Li_2S agrees with the findings of Moradabadi³⁵ et al., but differs from the conclusions drawn in two other studies.^{22,37} For example, Kim et al.²² found that the dominant carriers are V_{Li}^- and doubly charged positive S vacancies (V_S^{2+}), with formation energies of 1.31 eV. Alternatively, Mukherjee et al.³⁷ reported V_{Li}^- and hole polarons (p^+) as the predominant species, with formation energies (1.40 eV) similar to that of Kim et al. These

differences can be explained by the omission of interstitial defects in these earlier studies. The present calculations reveal that Li^+ interstitials are the lowest-energy positive charge carrier in Li_2S . Indeed, the removal Li^+ from our defect diagram (Figure 7) would shift the Fermi energy to a position similar to that reported by these earlier studies (1.3–1.4 eV), reflecting charge balance between V_{Li}^- and p^+/V_S^{2+} . (p^+ and V_S^{2+} are the same positive carriers reported in refs 22 and 37.) We emphasize that an accurate accounting of charge carrier concentrations can only be achieved if a comprehensive sampling of formation energies for all relevant defects—including interstitials—is performed.

The possibility for nonequilibrium carrier concentrations induced by rapid growth/dissolution of Li_2S during battery cycling prompts us to examine carriers beyond the ionic species described above, i.e., polarons. The stabilities of electron and hole polarons in Li_2S were explored by adding or removing a single electron from the computational cell, and by applying initial lattice distortions consistent with the presence/absence of localized charge on a S ion. For example, the presence of a hole polaron localized on a S ion (resulting in a charge state of S^{1-}) will reduce electrostatic attraction with nearest-neighbor Li ions and thereby increase Li–S distances. In contrast, the presence of an electron polaron will result in formation of a S^{3-} ion, which will more strongly attract adjacent Li^+ .

Regarding electron polarons, p^- , our attempts to localize an additional electron on a nominally S^{2-} ion were not successful. Several initial lattice distortions were attempted; nevertheless, in all cases the resulting relaxed structure resembled undistorted Li_2S , with the extra electron delocalized over the entire computational cell. In contrast, hole polarons, p^+ , do localize on S ions. The formation energy for p^+ is high, 1.95 eV (see Table 1 and Figure 7), with a correspondingly low equilibrium concentration of $4 \times 10^{-11} \text{ cm}^{-3}$. Furthermore, the localized hole is more stable than a delocalized hole by 0.07 eV. Figure 8 (top) shows the magnetization density isosurface for p^+ , indicating the presence of an unpaired electron localized on a S ion. The spatial distribution of this electron is consistent with that of a 3p orbital aligned toward a pair of nearest-neighbor Li ions, Figure 8 (bottom). The Li ions closest to the localized charge exhibit an enlarged Li–S distance of 2.78 Å, which should be compared to 2.46 Å in the absence of p^+ . (Two metastable p^+ with distinct local geometries were also identified, and are shown in Figure S3. These configurations are less stable by 13 and 68 meV, respectively.) The charge state of a S anion in the presence of a hole polaron was calculated using a Bader charge analysis.^{87,88} As expected, the total number of valence electrons, 7.2, is significantly smaller in the presence of p^+ than for a typical S^{2-} anion, wherein the number of electrons ranges from 7.9 to 8.0.

Our observation of self-trapping of holes on sulfur ions in Li_2S agrees with the calculations of Mukherjee et al.³⁷ Nevertheless, ref 22 reported a stability trend opposite to those of Mukherjee and the present calculations, with p^- being self-trapped and p^+ being unstable with respect to delocalization. Of course, the formation of p^- implies the existence of a S^{3-} anion, which our intuition suggests would be highly unstable. Moreover, the charge density plot used in ref 22 to substantiate the formation of S^{3-} does not show a distribution consistent with occupation of a 4s orbital, calling into question whether localization of an additional electron has occurred.

Finally, the formation of S_2^{2-} dimers was also investigated by introducing two neutral Li vacancies, V_{Li}^0 , or by removing two

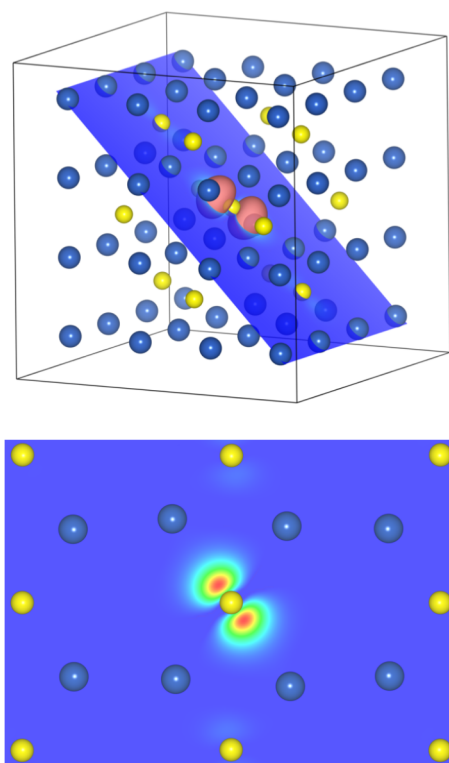


Figure 8. (Top) Magnetization density isosurface for the hole polaron in Li_2S . (Bottom) Contour plot of the magnetization density in a (110) plane. Red and blue areas represent magnetization densities of 0.06 and 0 e/bohr^3 , respectively.

electrons (equivalent to the introduction of two p^+) from the simulation cell. These calculations were motivated by the presence of S_2^{2-} dimers in iron pyrite, FeS_2 , where the S–S distance is 2.16 Å.⁸⁹ Dimer formation was induced by initially shortening the distance between adjacent S ions. Figure S4 illustrates the geometries of these relaxed S_2^{2-} dimers. The resulting S_2^{2-} dimers exhibited S–S distances of 2.10–2.13 Å. For both scenarios, formation of S_2^{2-} was energetically preferred over the formation of isolated vacancies or hole polarons. For example, the formation energy of two V_{Li}^0 and S_2^{2-} is 2.37 eV, while the sum of two single V_{Li}^0 is much higher, 4.86 eV. Similarly, E_f for two p^+ and a S_2^{2-} is 2.62 eV, which is well below that for two p^+ , 3.90 eV. These data indicate that it is energetically favorable for p^+ to localize as pairs on covalently bonded S_2^{2-} dimers. If the charging process involves an initial delithiation step, then the formation of S_2^{2-} dimers could constitute a portion of that reaction pathway.

Charge Carrier Mobility in Li_2S . The mobilities of Li^+ , V_{Li}^- , and p^+ were evaluated in the adiabatic limit using the HSE $_{\alpha}$ functional and the CI-NEB. Figure 9 shows the minimum energy pathways associated with the migration of these carriers.

In the case of Li^+ , two migration mechanisms were examined between neighboring interstitial sites, a simple interstitial hop, and interstitialcy diffusion. The interstitialcy mechanism corresponds to a Li^+ migrating toward an occupied Li site, while the ion occupying that site simultaneously hops to a neighboring interstitial position.⁹⁰ Our calculations predict that the interstitialcy mechanism has a much lower energy barrier ($E_a = 0.52$ eV) than the interstitial process ($E_a = 1.86$ eV). Based on these activation energies, the corresponding mobilities for these carriers are 6×10^{-10} and 2×10^{-32}

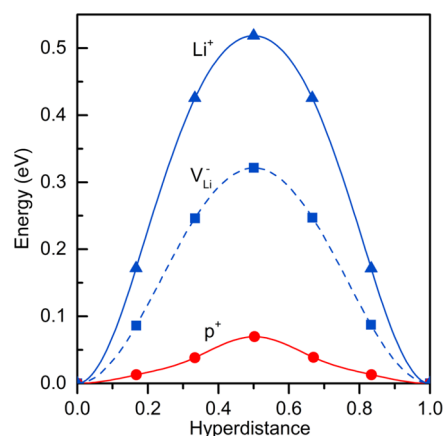


Figure 9. Calculated minimum energy pathways for migration of negative Li vacancies (V_{Li}^-), positive lithium interstitials (Li^+), and hole polarons (p^+) in Li_2S .

$\text{cm}^2/(\text{V s})$, respectively. Moradabadi et al. calculated a Li^+ interstitial migration barrier of 0.47 eV using the PBE-GGA functional.³⁵

For V_{Li}^- migration, there is only one symmetry-distinct Li vacancy site, and only one migration pathway between nearest-neighbor sites was considered. The calculated barrier for V_{Li}^- migration, 0.32 eV, is 0.2 eV smaller than that for Li interstitials. This barrier yields a mobility of 1×10^{-6} $\text{cm}^2/(\text{V s})$, which is approximately 4 orders of magnitude larger than that for Li^+ mobility. Our calculated energy barrier (evaluated using the HSE $_{48}$ functional) is in very good agreement with those reported by earlier studies employing the semilocal PBE-GGA functional ($E_a = 0.29$ and 0.27 eV)^{34,35} and the HSE06 hybrid functional ($E_a = 0.29$ eV).³⁷

For hole polarons, a very small activation energy of 0.08 eV was calculated for hopping between adjacent S ions. (The corresponding mobility is 3×10^{-2} $\text{cm}^2/(\text{V s})$.) This value is well-matched to that of a previous study that predicted a hopping barrier of 0.09 eV.³⁷ The predicted hopping barrier is much smaller than that observed for p^+ migration in Li_2O_2 , Na_2O_2 , and NaO_2 , where typical barriers are several tenths of an eV.^{30,61} On the other hand, the behavior of p^+ in Li_2S is similar to that of hole polarons in MgO, which were reported to have a barrier of only 0.11 eV and mobility of 6×10^{-3} $\text{cm}^2/(\text{V s})$.⁶⁰ These data suggest that hole transport in Li_2S can be more facile than in the discharge products of, e.g., metal–air batteries.

cDFT calculations confirm that both electron and hole polaron transfer reactions are adiabatic ($\kappa = 1$); therefore, the results from HSE-NEB calculations can be used with confidence. Moreover, the barrier for hopping of p^+ estimated using cDFT, 0.03 eV, differs only by 50 meV from the corresponding HSE $_{\alpha}$ -NEB value described above. Aside from this small difference in the barriers, the rates, mobilities, and conductivities predicted by both approaches (either HSE $_{\alpha}$ -NEB + harmonic transition state theory or cDFT + Marcus theory) are equal.

While we were unable to localize the electron polaron using HSE $_{\omega}$, localization of p^- can be achieved with cDFT. [We emphasize, however, that cDFT does not allow for an estimate of the self-trapping energy of p^- , and our earlier conclusion (based on HSE calculations) that electron polarons do not prefer to localize in Li_2S remains valid.] Nevertheless, cDFT does provide an opportunity to assess the mobility of p^- : These calculations yield a hopping barrier of 0.20 eV and rate constant

of $4.3 \times 10^8 \text{ s}^{-1}$, Table 1. Comparing the barriers and charge transfer rates in Table 1 for hole ($6.0 \times 10^{10} \text{ s}^{-1}$) and electron ($4.3 \times 10^8 \text{ s}^{-1}$) polarons, it is apparent that hole polarons are the most mobile electronic carriers in Li_2S .

Conductivity and Diffusion Length in Li_2S . Table 2 summarizes the transport properties of the three relevant defects in Li_2S identified here— Li^+ , V_{Li}^- , and p^+ —and for comparison revisits the dominant defect chemistry for the peroxides, Li_2O_2 and Na_2O_2 .^{30,61} The individual contributions of these carriers to the equilibrium ionic and electronic conductivity of Li_2S are evaluated in terms of their concentrations and mobilities, $\sigma = qC\mu$. V_{Li}^- exhibits the highest conductivity of the possible carriers in Li_2S , $6 \times 10^{-17} \text{ S/cm}$. Its conductivity is 2–3 orders of magnitude larger than Li^+ interstitials, and for the analogous cation vacancies in Li_2O_2 and Na_2O_2 . This higher conductivity results from a combination of relatively larger concentrations and mobilities of V_{Li}^- in Li_2S . Nevertheless, a conductivity on the order of 10^{-17} S/cm is an extremely low value. In practice, however, the presence of a higher, nonequilibrium carrier concentration may be achieved due to the rapid formation/dissolution of Li_2S during battery operation. Measurements of the ionic conductivity of Li_2S would be very helpful in identifying these nonequilibrium effects.

Regarding electronic conductivity in Li_2S , the negligible equilibrium concentration of p^+ , $4 \times 10^{-11} \text{ cm}^{-3}$, results in an extremely low (effectively zero) conductivity, $2 \times 10^{-30} \text{ S/cm}$. This conductivity is 10 orders of magnitude smaller than in the peroxides,^{30,61} and approaches the value estimated for MgO , 3×10^{-36} .⁶⁰ Although p^+ in Li_2S have relatively high mobilities, their low concentration offsets the benefits conveyed by these mobilities. Strategies for increasing the carrier concentration could exploit the moderate mobility of p^+ to improve the electronic conductivity.^{32,91}

We next consider whether the diffusivity and mobility of the dominant charge carriers in Li_2S are sufficient to access the full capacity of a Li–S cell. To determine this, a target S loading of 6 mg/cm^2 is adopted (as discussed above), and we further assume all S is reduced during discharge and forms a uniform film of Li_2S that covers the cathode support. Based on the density of Li_2S , such a film will have a thickness of approximately $50 \mu\text{m}$. During charging, charge transport through this film will be necessary; Table 2 summarizes whether the identified carriers have sufficient mobility to transit the film, assuming charging rates of 1C, C/5, and C/10. The data reveal that both V_{Li}^- and p^+ have adequate mobility to cross the film for all rates considered (based on their respective diffusion coefficients). Similarly, the drift length (assuming a voltage drop of 0.1 V across the Li_2S film) is sufficient to accommodate a $50 \mu\text{m}$ film. (The drift length is twice larger than the diffusion length.) In contrast, for all rates considered, the mobility of Li^+ interstitials is too small to contribute to charge transport across these relatively thick films.

These data indicate that the mobilities of V_{Li}^- and p^+ in Li_2S are sufficient to enable high active-material loadings (and high capacity) in Li–S cells. Thus, it is the low equilibrium concentration of carriers that is the primary limitation to effective charge transport. In an earlier study, we explored electrical conductivity limitations in Li_2O_2 in the related Li– O_2 system. There, a cathode conductivity of 10^{-11} S/cm was suggested as a target for achieving efficient operation.³⁰ Adopting that value here, and using the calculated mobility for p^+ , we determine that a carrier concentration of 10^8 cm^{-3} is

required to achieve the conductivity target. This concentration is 19 orders of magnitude larger than the equilibrium p^+ concentration listed in Table 1.

DISCUSSION

It is worthwhile to reexamine the previous experimental and theoretical studies of the electronic structure and polaron mobility in α -S. First, α -S is a molecular solid formed by S_8 rings that interact weakly through van der Waals forces. Thus, many of the electronic properties of α -S can be roughly understood from the molecular S_8 vapor phase. Indeed, the photoemission data for α -S and molecular S_8 are nearly identical,^{75,92,93} apart from the broadening of the lines in the former. As expected in a molecular solid formed by such small S_8 units, the electron–hole interactions are very large. Thus, the molecular excitonic peaks observed in optical absorption experiments in the ~ 3 – 5 eV range lie far below the photoemission gap, which is estimated to be close to 8 – 9 eV .⁹³

Consistent with its molecular nature, the dispersion of the bands in α -S is expected to be very small. Based on optical experiments, Spear and co-workers appraised the valence band bandwidth to be 0.80 eV , while the conduction band only spanned 0.01 eV .^{80,92} As shown here, the localization energies for hole polarons are positive (i.e., unfavorable), while localization of electron polarons is favored. In fact, free hole polarons (i.e., hole polarons not bonded to any defect) have not been observed in α -S, while free electron polarons have been detected with a polaron binding energy of 0.48 eV .^{75,80} As mentioned earlier, this energy is in good agreement with the value calculated in the present study, 0.42 eV .

As described above, our calculations predict that hole polarons in S cannot be localized on a single bond or S_8 ring. This leads us to conclude that hole conduction in sulfur is not polaronic in nature. This conclusion is consistent with experimental conductivity studies, which show that the hole lifetime in S is less than 20 ns , and that hole transfer is categorized as narrow band conduction rather than hopping.⁷⁶ In the band conduction regime, cDFT coupled with Marcus theory and DFT with transition state theory are inadequate to characterize the conduction mechanism and conductivity. Instead, hole transfer in S should be treated with nonadiabatic quantum dynamics based on the time-dependent Schrödinger equation. This approach naturally includes all possible conduction mechanisms without predefined assumptions. Along these lines, using Ehrenfest dynamics we observed that an initially localized hole polaron (on a single S_8 ring) delocalizes within 10 fs onto p-type orbitals spread across all atoms in the simulation cell (without changes in S–S bond lengths). These calculations agree well with the experimental results that show that holes in sulfur are conducted via a band mechanism, rather than via polaron hopping.

Several groups studied electron and hole diffusion in α -S during the 1960s.^{76,80} These studies concluded that at low temperatures (below 300 K) the diffusion of holes is controlled by a trapping mechanism; i.e., the holes are trapped at intrinsic defects in the α -S crystal and can diffuse with a $\sim 0.22 \text{ eV}$ activation barrier.^{76,80} At higher temperatures the trapping diffusion is saturated, and the hole transport changes to a lattice scattering regime (i.e., conduction through holes in the valence band).^{76,80} In the present work, we do not consider the transport of polarons bonded to any defect/trap, but instead focus on the diffusion of free polarons. In that context, it is most appropriate to compare our results to the higher-

temperature experiments. In this latter scenario, our prediction of delocalized holes agrees very well with the bandlike conduction observed in experiments.

An analysis of the formation energies of positively charged S_x ($x = 6-10$) rings relative to the formation energies of the neutral S_x rings (Figure S5) in α -S allows us to identify S_9 or S_{10} rings as the low-temperature traps observed experimentally^{76,80} (see the Supporting Information, Table S2 and Figure S6). In these two rings, localizing a positive charge is more favorable than the delocalized solution by 0.30 and 0.36 eV, respectively. Although the localization energy is larger for S_{10} rings, most likely the experimental signal of hole traps comes from S_9 rings, since their formation energy is much lower than that of S_{10} rings. Importantly, the calculated localization energy in S_9 rings, 0.30 eV, is very close to the experimental activation barrier, 0.22 eV.^{76,80} This finding confirms the hypothesis of Gill et al., who claimed that hole traps in α -S are formed from native defects.⁷⁶ (Other authors assumed that the hole traps originate from extrinsic defects.⁷⁷) Ehrenfest dynamics simulations on an initially localized hole on a S_9 ring reveal that the hole remains primarily localized to at least 23 fs (Figure S2). In contrast, a hole on a S_8 ring delocalizes completely within 10 fs. These direct electron–nuclear dynamics simulations suggest that hole polarons on S_9 defects are metastable, and can act as polaron traps.

Regarding the migration of electron polarons, two temperature regimes were again identified in experiments.^{76,80} At low temperatures (below 275 K), and similar to hole transport, a trapping mechanism with a ~ 0.40 eV barrier dominates. At higher temperatures, instead of passing to the lattice scatter regime, a free electron polaron hopping with a ~ 0.20 eV apparent activation barrier was reported as the dominant mechanism.^{76,80} Although the experimental barrier of ~ 0.20 eV is relatively close to the 0.37 eV predicted barrier in our diabatic model, the discrepancy between these values warrants additional discussion. First, the apparent activation energies from experiments are derived from Arrhenius slopes; therefore, any temperature-dependence in the pre-exponential factor is included in the barrier. This is noteworthy since in Marcus theory the prefactor is (weakly) temperature-dependent. Therefore, both computed and experimental estimates for the effective or apparent barrier from an Arrhenius analysis will include the temperature-dependence of the prefactor, and the apparent barrier will differ slightly from the barrier values reported in Table 1. Additional factors contributing to this discrepancy are the high concentration of intrinsic defects in the samples (10^{14} electron traps per cm^{-3} in the purest vapor grown samples) and the reported 15% error in the experimental estimation of the barriers.

To identify the electron polaron traps in α -S at low temperature, a similar analysis to the one used for hole polarons was conducted (see the Supporting Information). This analysis reveals that S_7 is the only S_x ring in α -S where localizing an electron is more favorable than in S_8 rings (by 0.38 eV). This energy difference is close to the estimate of 0.40 eV for the activation of electrons at low temperature made by Gill et al. based on measurements on vapor grown samples, corresponding to an electron hop from a S_7 to a S_8 ring.^{76,80}

Regarding Li_2S , our hybrid functional calculations indicate that hole polarons localized on S ions are stable, while electron polarons are not. Using cDFT, we can nevertheless force the localization of both hole and electron polarons and subsequently evaluate their migration barriers. The values

reported in Table 1 indicate that electron polaron transfer in Li_2S is much slower than hole transfer, mainly due to the larger reorganization energy required for migration of electron polarons. Based on other recent DFT calculations, hole polaron migration is also predicted to be much faster in Li_2S ,³⁶ a possible intermediate product in Li–S batteries. Taken together, these experimental and computational studies suggest that hole transport can be fast in α -S, Li_2S , and Li_2S_2 ; this observation implies that the performance of Li–S batteries can be improved (via enhanced electronic transport) by increasing the concentration of holes in these redox end members.

CONCLUSIONS

Understanding charge transport mechanisms in sulfur and Li_2S is a prerequisite for improving the capacity, efficiency, and cycle life of Li–S batteries. In α -S, these mechanisms have remained a matter of debate for more than 4 decades. The present study clarifies these mechanisms—in both the adiabatic and non-adiabatic charge transfer regimes—by employing a combination of hybrid-functional-based and constrained density functional theory calculations. The most significant outcomes of these calculations are summarized below.

Charged defects in both α -S and Li_2S are predicted to have high formation energies, resulting in negligible equilibrium carrier concentrations. In contrast, both compounds exhibit high mobilities for a subset of these carriers: in α -S, electron polarons and delocalized holes are the most mobile, whereas Li vacancies and hole polarons dominate in Li_2S . Importantly, analysis of the drift length for these species reveals that they have sufficient mobility to transit α -S and Li_2S films with thicknesses consistent with the JCESR sulfur loading targets. Thus, strategies to improve the conductivity of these materials should focus on increasing carrier concentrations beyond their equilibrium values.

In α -S, our calculations demonstrate that electrons can localize into polarons. Polaronic transfer within a single S_8 ring is predicted to be fast (10^{11} s^{-1}) and adiabatic. In contrast, polaron hopping between two adjacent S_8 rings is nonadiabatic, and much slower (10^4 s^{-1}). Neglecting nonadiabaticity, as is commonly done in DFT and transition state theory calculations, would overestimate these rate constants (and consequently also the mobility and the conductivity) by 2 orders of magnitude. This gap highlights the importance of going beyond the Born–Oppenheimer approximation by including nonadiabatic effects in computational studies of charge transfer kinetics in battery materials. Computational methods that combine cDFT with Marcus theory can treat both adiabatic and nonadiabatic charge transfer on equal footing, and are thus well-suited for these types of investigations.

Although electron polarons are stable in α -S, hole polarons are not. Instead, hole transport is expected to follow a bandlike mechanism, as suggested by experiments. The formation of delocalized holes in the valence band was confirmed by Ehrenfest dynamics, which show that an initially localized hole becomes delocalized across the entire computational cell within 10 fs, without changes in geometries. Furthermore, our calculations identify S_9 and S_7 rings as the defects that respectively trap holes and electrons in α -S, thus resolving a long-standing question regarding the nature of charge traps in this system.

In Li_2S , the highest-concentration carriers are ionic species, negative Li vacancies and positive Li interstitials. Of these, only vacancies have sufficient mobility to transit Li_2S films with

thicknesses consistent with the JCESR S loading target. Regarding electronic carriers in Li_2S , hole polarons are predicted to form, and to be more stable and mobile than electron polarons. Their transport can be categorized as adiabatic, and their mobilities are more than 2 orders of magnitude larger than for vacancy migration.

■ ASSOCIATED CONTENT

📄 Supporting Information

The Supporting Information is available free of charge on the ACS Publications website at DOI: [10.1021/acs.chemmater.7b04618](https://doi.org/10.1021/acs.chemmater.7b04618).

Bandgap of Li_2S as a function of exact exchange percentage in HSE, formulas for the adiabaticity correction, calculation of the coupling constant elements, Ehrenfest dynamics calculations, calculated diffusivity of defects at room temperature, structures and magnetization density plots of metastable hole polarons and S_2^{2-} dimers in Li_2S , and analysis of hole and electron polaron traps in $\alpha\text{-S}$. (PDF)

■ AUTHOR INFORMATION

Corresponding Author

*E-mail: djsiege@umich.edu. Phone: +1 (734) 764-4808.

ORCID

Haesun Park: 0000-0001-6266-8151

Marko Melander: 0000-0001-7111-1603

Donald J. Siegel: 0000-0001-7913-2513

Author Contributions

[○]H.P., N.K., and M.M. contributed equally.

Notes

The authors declare no competing financial interest.

■ ACKNOWLEDGMENTS

This work was supported as part of the Joint Center for Energy Storage Research (JCESR), an Energy Innovation Hub funded by the U.S. Department of Energy, Office of Science, and Basic Energy Sciences. The authors acknowledge the EU H2020 FET Open project Salbage (# 766581) and the Villum Foundation for support through the Mat4Bat project (# 10096) and the Visiting Professor Program. The Nordea Foundation's Residence Program is also acknowledged for support for D.J.S. during his stay at DTU Energy. M.M. acknowledges the grant from Alfred Kordelin Foundation as well as computer resources from CSC—IT Center for Science in Espoo, Finland.

■ REFERENCES

- (1) Seh, Z. W.; Sun, Y.; Zhang, Q.; Cui, Y. Designing high-energy lithium-sulfur batteries. *Chem. Soc. Rev.* **2016**, *45*, 5605–5634.
- (2) Pang, Q.; Liang, X.; Kwok, C. Y.; Nazar, L. F. Advances in lithium-sulfur batteries based on multifunctional cathodes and electrolytes. *Nat. Energy* **2016**, *1*, 16132.
- (3) Cheng, L.; Curtiss, L. A.; Zavadil, K. R.; Gewirth, A. A.; Shao, Y.; Gallagher, K. G. Sparingly Solvating Electrolytes for High Energy Density Lithium-Sulfur Batteries. *ACS Energy Lett.* **2016**, *1*, 503–509.
- (4) Manthiram, A.; Chung, S.-H.; Zu, C. Lithium-Sulfur Batteries: Progress and Prospects. *Adv. Mater.* **2015**, *27*, 1980–2006.
- (5) Bruce, P. G.; Freunberger, S. A.; Hardwick, L. J.; Tarascon, J.-M. Li-O₂ and Li-S batteries with high energy storage. *Nat. Mater.* **2012**, *11*, 19–29.

- (6) Moon, S.; Jung, Y. H.; Jung, W. K.; Jung, D. S.; Choi, J. W.; Kim, D. K. Encapsulated Monoclinic Sulfur for Stable Cycling of Li-S Rechargeable Batteries. *Adv. Mater.* **2013**, *25*, 6547–6553.

- (7) Ji, X.; Lee, K. T.; Nazar, L. F. A highly ordered nanostructured carbon-sulphur cathode for lithium-sulphur batteries. *Nat. Mater.* **2009**, *8*, 500–506.

- (8) Zheng, G.; Yang, Y.; Cha, J. J.; Hong, S. S.; Cui, Y. Hollow Carbon Nanofiber-Encapsulated Sulfur Cathodes for High Specific Capacity Rechargeable Lithium Batteries. *Nano Lett.* **2011**, *11*, 4462–4467.

- (9) Zhang, C.; Wu, H. B.; Yuan, C.; Guo, Z.; Lou, X. W. Confining Sulfur in Double-Shelled Hollow Carbon Spheres for Lithium-Sulfur Batteries. *Angew. Chem., Int. Ed.* **2012**, *51*, 9592–9595.

- (10) Zhou, G.; Zhao, Y.; Manthiram, A. Dual-Confining Flexible Sulfur Cathodes Encapsulated in Nitrogen-Doped Double-Shelled Hollow Carbon Spheres and Wrapped with Graphene for Li-S Batteries. *Adv. Energy Mater.* **2015**, *5*, 1402263.

- (11) Park, H.; Siegel, D. J. Tuning the Adsorption of Polysulfides in Lithium-Sulfur Batteries with Metal-Organic Frameworks. *Chem. Mater.* **2017**, *29*, 4932–4939.

- (12) Seo, D. M.; Borodin, O.; Han, S.-D.; Boyle, P. D.; Henderson, W. A. Electrolyte Solvation and Ionic Association II. Acetonitrile-Lithium Salt Mixtures: Highly Dissociated Salts. *J. Electrochem. Soc.* **2012**, *159*, A1489–A1500.

- (13) Dokko, K.; Tachikawa, N.; Yamauchi, K.; Tsuchiya, M.; Yamazaki, A.; Takashima, E.; Park, J.-W.; Ueno, K.; Seki, S.; Serizawa, N.; Watanabe, M. Solvate Ionic Liquid Electrolyte for Li-S Batteries. *J. Electrochem. Soc.* **2013**, *160*, A1304–A1310.

- (14) Ueno, K.; Park, J.-W.; Yamazaki, A.; Mandai, T.; Tachikawa, N.; Dokko, K.; Watanabe, M. Anionic Effects on Solvate Ionic Liquid Electrolytes in Rechargeable Lithium-Sulfur Batteries. *J. Phys. Chem. C* **2013**, *117*, 20509–20516.

- (15) Cuisinier, M.; Cabelguen, P. E.; Adams, B. D.; Garsuch, A.; Balasubramanian, M.; Nazar, L. F. Unique behaviour of nonsolvents for polysulphides in lithium-sulphur batteries. *Energy Environ. Sci.* **2014**, *7*, 2697–2705.

- (16) Yamada, Y.; Yamada, A. Review—Superconcentrated Electrolytes for Lithium Batteries. *J. Electrochem. Soc.* **2015**, *162*, A2406–A2423.

- (17) Younesi, R.; Veith, G. M.; Johansson, P.; Edstrom, K.; Vegge, T. Lithium salts for advanced lithium batteries: Li-metal, Li-O₂, and Li-S. *Energy Environ. Sci.* **2015**, *8*, 1905–1922.

- (18) Zhang, S.; Ueno, K.; Dokko, K.; Watanabe, M. Recent Advances in Electrolytes for Lithium-Sulfur Batteries. *Adv. Energy Mater.* **2015**, *5*, 1500117.

- (19) Das, S.; Ngene, P.; Norby, P.; Vegge, T.; de Jongh, P. E.; Blanchard, D. All-Solid-State Lithium-Sulfur Battery Based on a Nanoconfined LiBH₄ Electrolyte. *J. Electrochem. Soc.* **2016**, *163*, A2029–A2034.

- (20) Lee, C.-W.; Pang, Q.; Ha, S.; Cheng, L.; Han, S.-D.; Zavadil, K. R.; Gallagher, K. G.; Nazar, L. F.; Balasubramanian, M. Directing the Lithium-Sulfur Reaction Pathway via Sparingly Solvating Electrolytes for High Energy Density Batteries. *ACS Cent. Sci.* **2017**, *3*, 605–613.

- (21) Helen, M.; Reddy, M. A.; Diemant, T.; Golla-Schindler, U.; Behm, R. J.; Kaiser, U.; Fichtner, M. Single step transformation of sulphur to Li₂S₂/Li₂S in Li-S batteries. *Sci. Rep.* **2015**, *5*, 12146.

- (22) Kim, B. S. D.-H.; Lee, M. S. B.; Park, K.-Y.; Kang, K. First-principles Study on the Charge Transport Mechanism of Lithium Sulfide (Li₂S) in Lithium-Sulfur Batteries. *Chem. - Asian J.* **2016**, *11*, 1288–1292.

- (23) Park, H.; Koh, H. S.; Siegel, D. J. First-Principles Study of Redox End Members in Lithium-Sulfur Batteries. *J. Phys. Chem. C* **2015**, *119*, 4675–4683.

- (24) Albertus, P.; Girishkumar, G.; McCloskey, B.; Sánchez-Carrera, R. S.; Kozinsky, B.; Christensen, J.; Luntz, A. C. Identifying Capacity Limitations in the Li/Oxygen Battery Using Experiments and Modeling. *J. Electrochem. Soc.* **2011**, *158*, A343–A351.

- (25) Chen, J.; Hummelshøj, J. S.; Thygesen, K. S.; Myrdal, J. S. G.; Nørskov, J. K.; Vegge, T. The role of transition metal interfaces on the

electronic transport in lithium–air batteries. *Catal. Today* **2011**, *165*, 2–9.

(26) Viswanathan, V.; Thygesen, K. S.; Hummelshøj, J. S.; Nørskov, J. K.; Girishkumar, G.; McCloskey, B. D.; Luntz, A. C. Electrical conductivity in Li₂O₂ and its role in determining capacity limitations in non-aqueous Li–O₂ batteries. *J. Chem. Phys.* **2011**, *135*, 214704.

(27) Das, S. K.; Xu, S.; Emwas, A.-H.; Lu, Y. Y.; Srivastava, S.; Archer, L. A. High energy lithium-oxygen batteries - transport barriers and thermodynamics. *Energy Environ. Sci.* **2012**, *5*, 8927–8931.

(28) Lu, Y.-C.; Shao-Horn, Y. Probing the Reaction Kinetics of the Charge Reactions of Nonaqueous Li–O₂ Batteries. *J. Phys. Chem. Lett.* **2013**, *4*, 93–99.

(29) Luntz, A. C.; Viswanathan, V.; Voss, J.; Varley, J. B.; Nørskov, J. K.; Scheffler, R.; Speidel, A. Tunneling and Polaron Charge Transport through Li₂O₂ in Li–O₂ Batteries. *J. Phys. Chem. Lett.* **2013**, *4*, 3494–3499.

(30) Radin, M. D.; Siegel, D. J. Charge transport in lithium peroxide: relevance for rechargeable metal-air batteries. *Energy Environ. Sci.* **2013**, *6*, 2370–2379.

(31) Viswanathan, V.; Nørskov, J. K.; Speidel, A.; Scheffler, R.; Gowda, S.; Luntz, A. C. Li–O₂ Kinetic Overpotentials: Tafel Plots from Experiment and First-Principles Theory. *J. Phys. Chem. Lett.* **2013**, *4*, 556–560.

(32) Radin, M. D.; Monroe, C. W.; Siegel, D. J. Impact of Space-Charge Layers on Sudden Death in Li/O₂ Batteries. *J. Phys. Chem. Lett.* **2015**, *6*, 3017–3022.

(33) Fan, F. Y.; Carter, W. C.; Chiang, Y.-M. Mechanism and Kinetics of Li₂S Precipitation in Lithium–Sulfur Batteries. *Adv. Mater.* **2015**, *27*, 5203–5209.

(34) Lee, B.; Kim, J.; Yoon, G.; Lim, H.-D.; Choi, I.-S.; Kang, K. Theoretical Evidence for Low Charging Overpotentials of Superoxide Discharge Products in Metal–Oxygen Batteries. *Chem. Mater.* **2015**, *27*, 8406–8413.

(35) Moradabadi, A.; Kaghazchi, P. Thermodynamics and kinetics of defects in Li₂S. *Appl. Phys. Lett.* **2016**, *108*, 213906.

(36) Liu, Z.; Balbuena, P. B.; Mukherjee, P. P. Revealing Charge Transport Mechanisms in Li₂S₂ for Li–Sulfur Batteries. *J. Phys. Chem. Lett.* **2017**, *8*, 1324–1330.

(37) Liu, Z.; Balbuena, P. B.; Mukherjee, P. P. Hole Polaron Diffusion in the Final Discharge Product of Lithium–Sulfur Batteries. *J. Phys. Chem. C* **2017**, *121*, 17169–17175.

(38) Henkelman, G.; Jonsson, H. Improved tangent estimate in the nudged elastic band method for finding minimum energy paths and saddle points. *J. Chem. Phys.* **2000**, *113*, 9978–9985.

(39) Henkelman, G.; Uberuaga, B. P.; Jónsson, H. A climbing image nudged elastic band method for finding saddle points and minimum energy paths. *J. Chem. Phys.* **2000**, *113*, 9901–9904.

(40) Sheppard, D.; Terrell, R.; Henkelman, G. Optimization methods for finding minimum energy paths. *J. Chem. Phys.* **2008**, *128*, 134106.

(41) Kuznetsov, A. M.; Ulstrup, J. *Electron transfer in chemistry and biology: an introduction to the theory*; Wiley, 1999.

(42) Marcus, R. A. On the theory of oxidation-reduction reactions involving electron transfer. *J. Chem. Phys.* **1956**, *24*, 966–978.

(43) Marcus, R. A.; Sutin, N. Electron transfers in chemistry and biology. *Biochim. Biophys. Acta, Rev. Bioenerg.* **1985**, *811*, 265–322.

(44) Heyd, J.; Scuseria, G. E.; Ernzerhof, M. Hybrid functionals based on a screened Coulomb potential. *J. Chem. Phys.* **2003**, *118*, 8207–8215.

(45) Krukau, A. V.; Vydrov, O. A.; Izmaylov, A. F.; Scuseria, G. E. Influence of the exchange screening parameter on the performance of screened hybrid functionals. *J. Chem. Phys.* **2006**, *125*, 224106.

(46) Song, M.-K.; Zhang, Y.; Cairns, E. J. A Long-Life, High-Rate Lithium/Sulfur Cell: A Multifaceted Approach to Enhancing Cell Performance. *Nano Lett.* **2013**, *13*, 5891–5899.

(47) Eroglu, D.; Zavadil, K. R.; Gallagher, K. G. Critical Link between Materials Chemistry and Cell-Level Design for High Energy Density and Low Cost Lithium-Sulfur Transportation Battery. *J. Electrochem. Soc.* **2015**, *162*, A982–A990.

(48) Kresse, G.; Furthmüller, J. Efficient iterative schemes for ab initio total-energy calculations using a plane-wave basis set. *Phys. Rev. B: Condens. Matter Mater. Phys.* **1996**, *54*, 11169–11186.

(49) Kresse, G.; Furthmüller, J. Efficiency of ab-initio total energy calculations for metals and semiconductors using a plane-wave basis set. *Comput. Mater. Sci.* **1996**, *6*, 15–50.

(50) Adams, A. R.; Gibbons, D. J.; Spear, W. E. Electron hopping transport in orthorhombic S crystals. *Solid State Commun.* **1964**, *2*, 387–389.

(51) Rettig, S. J.; Trotter, J. Refinement of the structure of orthorhombic sulfur, α -S₈. *Acta Crystallogr., Sect. C: Cryst. Struct. Commun.* **1987**, *43*, 2260–2262.

(52) Murnaghan, F. D. The Compressibility of Media under Extreme Pressures. *Proc. Natl. Acad. Sci. U. S. A.* **1944**, *30*, 244–247.

(53) Buehrer, W.; Altorfer, F.; Mesot, J.; Bill, H.; Carron, P.; Smith, H. G. Lattice dynamics and the diffuse phase transition of lithium sulphide investigated by coherent neutron scattering. *J. Phys.: Condens. Matter* **1991**, *3*, 1055.

(54) Kresse, G.; Joubert, D. From ultrasoft pseudopotentials to the projector augmented-wave method. *Phys. Rev. B: Condens. Matter Mater. Phys.* **1999**, *59*, 1758–1775.

(55) Blochl, P. E. PROJECTOR AUGMENTED-WAVE METHOD. *Phys. Rev. B: Condens. Matter Mater. Phys.* **1994**, *50*, 17953–17979.

(56) Pacchioni, G. Modeling doped and defective oxides in catalysis with density functional theory methods: Room for improvements. *J. Chem. Phys.* **2008**, *128*, 182505.

(57) Alkauskas, A.; Broqvist, P.; Pasquarello, A. Defect levels through hybrid density functionals: Insights and applications. *Phys. Status Solidi B* **2011**, *248*, 775–789.

(58) Lambrecht, W. R. L. Which electronic structure method for the study of defects: A commentary. *Phys. Status Solidi B* **2011**, *248*, 1547–1558.

(59) Li, S.; Liu, J.; Liu, B. First-Principles Study of the Charge Transport Mechanisms in Lithium Superoxide. *Chem. Mater.* **2017**, *29*, 2202–2210.

(60) Smith, J. G.; Naruse, J.; Hiramatsu, H.; Siegel, D. J. Intrinsic Conductivity in Magnesium-Oxygen Battery Discharge Products: MgO and MgO₂. *Chem. Mater.* **2017**, *29*, 3152–3163.

(61) Yang, S.; Siegel, D. J. Intrinsic Conductivity in Sodium–Air Battery Discharge Phases: Sodium Superoxide vs Sodium Peroxide. *Chem. Mater.* **2015**, *27*, 3852–3860.

(62) Komsa, H.-P.; Rantala, T. T.; Pasquarello, A. Finite-size supercell correction schemes for charged defect calculations. *Phys. Rev. B: Condens. Matter Mater. Phys.* **2012**, *86*, 045112.

(63) Van de Walle, C. G.; Neugebauer, J. First-principles calculations for defects and impurities: Applications to III-nitrides. *J. Appl. Phys.* **2004**, *95*, 3851–3879.

(64) Sulfur (S) dielectric constant, refractive index, orthorhombic alpha-modification. In *Non-Tetrahedrally Bonded Elements and Binary Compounds I*; Madelung, O., Rössler, U., Schulz, M., Eds.; Springer Berlin Heidelberg: Berlin, 1998; pp 1–5.

(65) Makov, G.; Payne, M. C. Periodic boundary conditions in ab initio calculations. *Phys. Rev. B: Condens. Matter Mater. Phys.* **1995**, *51*, 4014–4022.

(66) Hummelshøj, J. S.; Luntz, A. C.; Nørskov, J. K. Theoretical evidence for low kinetic overpotentials in Li–O₂ electrochemistry. *J. Chem. Phys.* **2013**, *138*, 034703.

(67) Loftager, S.; García-Lastra, J. M.; Vegge, T. A Density Functional Theory Study of the Ionic and Electronic Transport Mechanisms in LiFeBO₃ Battery Electrodes. *J. Phys. Chem. C* **2016**, *120*, 18355–18364.

(68) Wu, Q.; Van Voorhis, T. Direct optimization method to study constrained systems within density-functional theory. *Phys. Rev. A: At, Mol., Opt. Phys.* **2005**, *72*, 024502.

(69) Kaduk, B.; Kowalczyk, T.; Van Voorhis, T. Constrained Density Functional Theory. *Chem. Rev.* **2012**, *112*, 321–370.

(70) Melander, M.; Jónsson, E. O.; Mortensen, J. J.; Vegge, T.; García Lastra, J. M. Implementation of Constrained DFT for Computing

Charge Transfer Rates within the Projector Augmented Wave Method. *J. Chem. Theory Comput.* **2016**, *12*, 5367–5378.

(71) Mortensen, J. J.; Hansen, L. B.; Jacobsen, K. W. Real-space grid implementation of the projector augmented wave method. *Phys. Rev. B: Condens. Matter Mater. Phys.* **2005**, *71*, 035109.

(72) Enkovaara, J.; Rostgaard, C.; Mortensen, J. J.; Chen, J.; Dulak, M.; Ferrighi, L.; Gavnholt, J.; Glinsvad, C.; Haikola, V.; Hansen, H. A.; Kristoffersen, H. H.; Kuisma, M.; Larsen, A. H.; Lehtovaara, L.; Ljungberg, M.; Lopez-Acevedo, O.; Moses, P. G.; Ojanen, J.; Olsen, T.; Petzold, V.; Romero, N. A.; Stausholm-Møller, J.; Strange, M.; Tritsarolis, G. A.; Vanin, M.; Walter, M.; Hammer, B.; Häkkinen, H.; Madsen, G. K. H.; Nieminen, R. M.; Nørskov, J. K.; Puska, M.; Rantala, T. T.; Schiøtz, J.; Thygesen, K. S.; Jacobsen, K. W. Electronic structure calculations with GPAW: a real-space implementation of the projector augmented-wave method. *J. Phys.: Condens. Matter* **2010**, *22*, 253202.

(73) Perdew, J. P.; Burke, K.; Ernzerhof, M. Generalized Gradient Approximation Made Simple. *Phys. Rev. Lett.* **1996**, *77*, 3865–3868.

(74) Dolezalek, F. K.; Spear, W. E. Carrier recombination in orthorhombic sulphur. *J. Phys. Chem. Solids* **1975**, *36*, 819–825.

(75) Nitzki, V.; Stössel, W. Anisotropy of Electron and Hole Mobilities in Orthorhombic Sulphur Crystals. *Phys. Status Solidi B* **1970**, *39*, 309–316.

(76) Gill, W. D.; Street, G. B.; Macdonald, R. E. Transport properties of vapor grown orthorhombic sulfur crystals. *J. Phys. Chem. Solids* **1967**, *28*, 1517–1518.

(77) Adams, A. R.; Spear, W. E. The charge transport in orthorhombic sulphur crystals. *J. Phys. Chem. Solids* **1964**, *25*, 1113–1118.

(78) Neumann, H. Leitfähigkeit und dielektrische Hysteresis einiger Isolatoren und ihre Beeinflussung durch Röntgen- und γ -Strahlen. *Eur. Phys. J. A* **1927**, *45*, 717–748.

(79) Sproul, A. B.; Green, M. A. Improved value for the silicon intrinsic carrier concentration from 275 to 375 K. *J. Appl. Phys.* **1991**, *70*, 846–854.

(80) Gibbons, D. J.; Spear, W. E. Electron hopping transport and trapping phenomena in orthorhombic sulphur crystals. *J. Phys. Chem. Solids* **1966**, *27*, 1917–1925.

(81) Garcia-Lastra, J. M.; Mowbray, D. J.; Thygesen, K. S.; Rubio, A.; Jacobsen, K. W. Modeling nanoscale gas sensors under realistic conditions: Computational screening of metal-doped carbon nanotubes. *Phys. Rev. B: Condens. Matter Mater. Phys.* **2010**, *81*, 10.

(82) Jurchescu, O. D.; Baas, J.; Palstra, T. T. M. Effect of impurities on the mobility of single crystal pentacene. *Appl. Phys. Lett.* **2004**, *84*, 3061–3063.

(83) Munn, R. W.; Siebrand, W. Theory of electron-phonon interactions in organic crystals. Effect on charge carrier transport. *Discuss. Faraday Soc.* **1971**, *51*, 17–23.

(84) Silbey, R.; Munn, R. W. General theory of electronic transport in molecular crystals. I. Local linear electron–phonon coupling. *J. Chem. Phys.* **1980**, *72*, 2763–2773.

(85) Nitzki, V.; Stössel, W. Anisotropy of Electron and Hole Mobilities in Orthorhombic Sulphur Crystals. *Phys. Status Solidi B* **1970**, *39*, 309–316.

(86) Ashcroft, N. W.; Mermin, N. D. *Solid State Physics*; Holt, Rinehart and Winston, 1976.

(87) Henkelman, G.; Arnaldsson, A.; Jónsson, H. A fast and robust algorithm for Bader decomposition of charge density. *Comput. Mater. Sci.* **2006**, *36*, 354–360.

(88) Tang, W.; Sanville, E.; Henkelman, G. A grid-based Bader analysis algorithm without lattice bias. *J. Phys.: Condens. Matter* **2009**, *21*, 084204.

(89) Stevens, E. D.; DeLucia, M. L.; Coppens, P. Experimental observation of the effect of crystal field splitting on the electron density distribution of iron pyrite. *Inorg. Chem.* **1980**, *19*, 813–820.

(90) Tilley, R. J. D. Defects and Diffusion. In *Defects in Solids*; John Wiley & Sons, Inc., 2008; pp 205–250.

(91) Radin, M. D.; Monroe, C. W.; Siegel, D. J. How Dopants Can Enhance Charge Transport in Li₂O₂. *Chem. Mater.* **2015**, *27*, 839–847.

(92) Cook, B. E.; Spear, W. E. The optical properties of orthorhombic sulphur crystals in the vacuum ultraviolet. *J. Phys. Chem. Solids* **1969**, *30*, 1125–1134.

(93) Coppens, P.; Yang, Y. W.; Blessing, R. H.; Copper, W. F.; Larsen, F. K. The experimental charge distribution in sulfur containing molecules. Analysis of cyclic octasulfur at 300 and 100 K. *J. Am. Chem. Soc.* **1977**, *99*, 760–766.